Journal of Magnetism and Magnetic Materials 562 (2022) 169766

Contents lists available at ScienceDirect

Journal of Magnetism and Magnetic Materials

journal homepage: www.elsevier.com/locate/jmmm

Research article

Anomalous transverse effects in nodal line compounds Co_2TaX (X = Al, Ga)

P. Rambabu [a,b,1], Anusree C.V. [a,1], M. Manivel Raja [c], V. Kanchana [a,*]

[a] Department of Physics, Indian Institute of Technology Hyderabad, Kandi 502285, Sangareddy, Telangana, India
[b] Department of Pure and Applied Physics, Guru Ghasidas Vishwavidyalaya, Koni, Bilaspur, 495009, Chattisgarh, India
[c] Advanced Magnetic Group, Defence Metallurgical Research Laboratory, Kanchanbagh P.O- 500058, Hyderabad, Telangana, India

ARTICLE INFO

Keywords:
Spintronics
Berry curvature
Anomalous Hall effect
Anomalous Nernst effect
Magneto-optic Kerr effect

ABSTRACT

The magnetic ground state, electronic, and elastic properties of Co_2TaX (X = Al, Ga) are investigated using Density functional theory calculations. The compounds are found to possess mechanical and dynamical stability. Both the compounds exhibit nodal line features in the majority spin channel without the inclusion of spin-orbit coupling (SOC) and become gapped lines when SOC is added. The anomalous Hall effect and anomalous Nernst effect caused by Berry curvature are investigated. Within the region of $\pm 300meV$ around Fermi level, the maximum values of anomalous Hall conductivities (AHC) are −602.8 S/cm and −593.8 S/cm, while anomalous Nernst conductivities (ANC) are -4.989 $Am^{-1}K^{-1}$ and 4.934 $Am^{-1}K^{-1}$ respectively, for Co_2TaX (X = Al, Ga) compounds. Through the Heisenberg magnetic exchange interactions, the Curie temperatures (T_C) for both Co_2TaX (X = Al, Ga) compounds are calculated to be 560.7 K and 556.3 K within the mean-field approximation (MFA). The magneto-optical response is also examined, and the polar Kerr rotation angles for Co_2TaAl and Co_2TaGa at normal incidence were determined to be 0.11° and 1.35°, respectively. As a result, this study may pave the way for precise property engineering in real-world applications.

1. Introduction

Though the existence of Heusler alloys is more than a century after the discovery of ferromagnetic behavior in the intermetallic compound Cu_2MnAl by Fritz Heusler in 1903 [1], yet half-metallic ferromagnetic alloys have dragged much attention of the researchers worldwide because of their novel applications due to their unique physical properties. These half-metallic Heusler alloys are known to possess 100% spin polarization due to their conducting behavior in one spin channel and semiconducting/insulating behavior in the other spin channel. Hence they are expected to produce highly spin polarized currents [2] which are useful for spintronics applications. Shape memory alloys [3], thermoelectricity [4], topological insulators [5], superconductors [6,7], magneto-resistive devices [8], magnetic tunnel junctions [9], spin filters [10], spin-resonant tunneling diodes, spintronic transistors, and spin light-emitting diodes [11] are all potential applications for Heusler alloys. The full Heusler alloys with X_2YZ formula where X, Y are transition metals and Z is 'sp' element will crystallize into two prototype structures: a) Cu_2MnAl-type with space group $Fm\bar{3}m$ in which X, Y and Z atoms respectively occupy the positions (1/4, 1/4, 1/4), (1/2, 1/2, 1/2) and (0, 0, 0) and b) Hg_2CuTi-type with 4 inequivalent lattice sites with space group $F\bar{4}3m$ in which X, X′, Y and Z atoms respectively occupy the positions (0, 0, 0), (1/4, 1/4, 1/4), (1/2, 1/2, 1/2) and (3/4, 3/4, 3/4).

The magnetic Heusler compounds are a promising and adaptable class of materials that can be easily tailored for various properties. They can be grown as thin films and are discovered to have high Curie temperatures. They also have topological and magnetic properties in their band structure, making them a viable research platform for studying linear response effects such as anomalous Hall effect (AHE), anomalous Nernst effect (ANE), spin Hall conductivity (SHC) etc. As a result, the Heusler compounds may have greater uses in the contemporary electronic systems and gadgets due to their diverse set of features [12]. Recently, many research groups across the globe focus on Heusler alloys in search of colossal AHE as well as for ANE in these compounds. Extrinsic mechanisms such as side jump [13,14], skew scattering [15], and intrinsic mechanisms such as Berry curvature [16–20], and Karplus–Luttinger [21] generate AHE. In a study, a massive room temperature AHE was discovered in the Heusler compound Co_2MnAl [22], with an AHC value of almost 1300 S/cm. The compensated half-metallic Mn_2Ru_xGa [23] thin films were found to have an AHC value of 6673 S/cm in another investigation. The authors reported an AHC of 60 S/cm for Co_2TiGe Heusler half-metal in their study [24]. The Co_2TiSn [25] alloy has an AHC value of 284 S/cm. At 20 K, the authors reported AHC

* Corresponding author.
E-mail address: kanchana@phy.iith.ac.in (V. Kanchana).
[1] These authors contributed equally.

https://doi.org/10.1016/j.jmmm.2022.169766
Received 18 April 2022; Received in revised form 26 July 2022; Accepted 26 July 2022
Available online 9 August 2022

values of 55 S/cm for Co_2TiSi and 170 S/cm for Co_2TiGe compounds, respectively. Another study [26] found that the Co_2FeGe alloy has an AHC value of 100 S/cm. Khandy et al. theoretically reported the phase stability, electronic structure and half-metallic magnetism in Co_2TaZ (Z = Al, Ga, In) Heusler alloys and out of the two L21 and Hg_2CuTi-type phases, they found the L21 phase getting more stabilized in the studied compounds with 100% spin polarization [27]. Other theoretical studies on Co_2TaGa [28] and Co_2TaAl [29] compounds claim the Hg_2CuTi-type structure as the stable one theoretically. Because of the high spin polarizations in the ordered L21 structure and the high tolerances for the Co-related atomic disorder, it is determined that Co-based full-Heusler alloys are promising candidates as stable half-metallic ferromagnets with higher Curie temperatures and are worthy of further study [30]. The compounds studied in this research, Co_2TaAl [31,32] and Co_2TaGa, are ferromagnetic half metals that has no reports on anomalous transverse effects and magneto-optical response, which we intended to investigate in this paper.

Heusler alloys are one of the most appealing alternatives for spintronic applications due to 100% spin polarization and high ferromagnetic transition temperature. Heusler alloys have remarkable magneto-optical properties: the revelation of reasonable Kerr rotation for the half-Heusler PtMnSb (> 2.0° at ambient temperature and 5° at 80 K) for a 3d-based material [33] was completely unexpected. It demonstrated the technological significance of magneto-optics for this family of compounds as it attained a lot of attention since then [34].

The goal of this paper is to investigate the ground state magnetic properties using Heisenberg exchange interactions and Curie temperature (T_C) estimation via mean-field approximation. The structural and electronic properties are also probed in along with the linear response transverse effects like AHE and ANE. The mechanical and dynamical stability of the compounds have been ensured by the elastic properties and phonon dispersion studies. Besides, the polar magneto-optical Kerr effect has also been analyzed in these compounds.

2. Computational details

The magnetic, electronic and elastic characteristics of Co_2TaX (X = Al, Ga) compounds were investigated using Density Functional Theory (DFT). The projector-augmented wave (PAW) method [35], as implemented in Vienna Ab-Initio Simulation Package (VASP) [36,37], is used to account for electron–ion interactions. For sampling the Brillouin zone, we employed a 516 eV plane-wave energy cutoff and a k-point grid of 21 × 21 × 21 in the Monkhorst–Pack [38] method. Perdew, Burke, and Ernzerhof(PBE) [39] functional within the generalized-gradient approximation (GGA) is used to treat the system's exchange and correlations. The compounds' ionic relaxation is obtained up to a force convergence of 10^{-2} eV/Åand an electronic convergence of 10^{-6} eV. The spin-polarized relativistic Korringa–Kohn–Rostoker (SPR-KKR) package [40] is used to investigate the T_C using mean-field approximation through Heisenberg magnetic exchange interactions, with l_{max} = 3 for the full potential spin-polarized scalar relativistic Hamiltonian and a k-mesh of 35 × 35 × 35 for the Brillouin zone integration. The harmonic force constants are obtained from Density Functional Perturbation theory (DFPT) approach based on DFT force calculations implemented in VASP and then dynamical matrices are diagonalized to generate the phonon dispersion relation using PHONOPY [41] package, using a 2 × 2 × 2 supercell of primitive Co_2TaX (X = Al, Ga) with 16 Co, 8 Ta, and 8 X atoms, respectively, and a 2 × 2 × 2 k-mesh. Wannier90 [42] and wannier_tools [43] with a k-mesh of 301 × 301 × 301 are used to investigate anomalous Hall conductivity. The magneto-optical calculations are performed with the WANNIER90 package's BERRY module [18,44], which constructs an effective band interpolation technique using maximally localized Wannier functions [45,46].

Table 1
The optimized lattice constants in Å for Co_2TaX (X = Al, Ga) with the ground state energy along with their formation energies (E_f) in Hg_2CuTi and Cu_2MnAl-type structures. The experimental lattice constants in Å are also provided here. In Cu_2MnAl-type structure X, Y, and Z atoms occupy the Wyckoff positions (1/4, 1/4, 1/4), (1/2, 1/2, 1/2) and (0, 0, 0) and in Hg_2CuTi-type structure X, X', Y and Z atoms occupy the Wyckoff positions (0, 0, 0), (1/4, 1/4, 1/4), (1/2, 1/2, 1/2) and (3/4, 3/4, 3/4) respectively.

Compound	Structure	Phase	a (Å)	E_{tot} (eV)	E_f (eV)
Co_2TaAl	Hg_2CuTi	FM	5.979	−118.9493	−0.3412
		NM	5.964	−118.3547	–
	Cu_2MnAl	FM	5.943	−126.1655	−2.1459
		NM	5.922	−125.7422	–
	Experimental	FM	5.930	–	–
Co_2TaGa	Hg_2CuTi	FM	5.985	−114.9809	−0.196
		NM	5.969	−114.5053	–
	Cu_2MnAl	FM	5.944	−120.8439	−1.6631
		NM	5.923	−120.3947	–
	Experimental	–	–	–	–

3. Results and discussions

3.1. Ground state, electronic and magnetic properties

The compounds Co_2TaX (X = Al, Ga) are optimized in Hg_2CuTi and Cu_2MnAl-type structures for both ferromagnetic (FM) and nonmagnetic (NM) configurations. The optimized Volume–Energy curves for both the compounds for various structure types are shown in Fig. 1(c and d). The obtained lattice constants with their respective total energies for various configurations are shown in Table 1. Both the compounds are found to be in the FM L21 phase which takes a cubic face-centered Bravais lattice with the space group $Fm\bar{3}m$ (225) as depicted in Fig. 1(a). The formation energy (E_f) of the X_2YZ compound is given by the formula:

$$E_f = E^{tot}_{X_2YZ} - 2E_x - E_Y - E_Z \quad (1)$$

The E_f for both the compounds in FM phase for Cu_2MnAl and Hg_2CuTi-types are calculated and tabulated. From Table 1, it is evident that E_f is more negative for Cu_2MnAl-type for both the compounds, further supporting the stability of these compounds in the L21 phase. The compounds contain a total 16 atoms in its conventional cell whereas the primitive unit cell contains only 4 atoms. The atoms Co, Ta and X respectively occupy (1/4, 1/4, 1/4), (1/2, 1/2, 1/2) and (0, 0, 0) positions. The corresponding Brillouin zone (BZ) is shown in Fig. 1(b). The lattice constants obtained after optimization are in close agreement with its experimental counterparts [32], which can be seen from Table 1. The Slater–Pauling [47] rule, which the L21 ferromagnetic half metals exhibit in general, is given by equation:

$$M_t = Z_t - 24 \quad (2)$$

where Z_t and M_t are the total number of valence electrons and total magnetic moment in μ_B per f.u., respectively. The total magnetic moment of the investigated compounds Co_2TaX (X = Al, Ga) are 1.99 μ_B and 1.97 μ_B, respectively, which is close to $2\mu_B$, indicating that they are half metals and follow the Slater–Pauling rule. As shown in Table 2, the moment on the Co-atom in both the compounds Co_2TaX (X = Al, Ga) is 1.01 μ_B, which contributes to the magnetization in these compounds. The experimental magnetic moment on Co_2TaAl per formula unit is 1.50 μ_B[31] which is less than that of the calculated magnetic moment 1.99 μ_B and the reason for this less moment may be attributed to the presence of B2-type or DO_3-type atomic disorders [48] in the experimentally prepared sample. A similar situation has been observed in many other Heusler compounds [11,49–52]

Fig. 2(a,b) depicts the spin polarized band structures of both Co_2TaX (X = Al, Ga) compounds. The majority and minority spin bands are represented by the solid black and dashed red lines. The majority

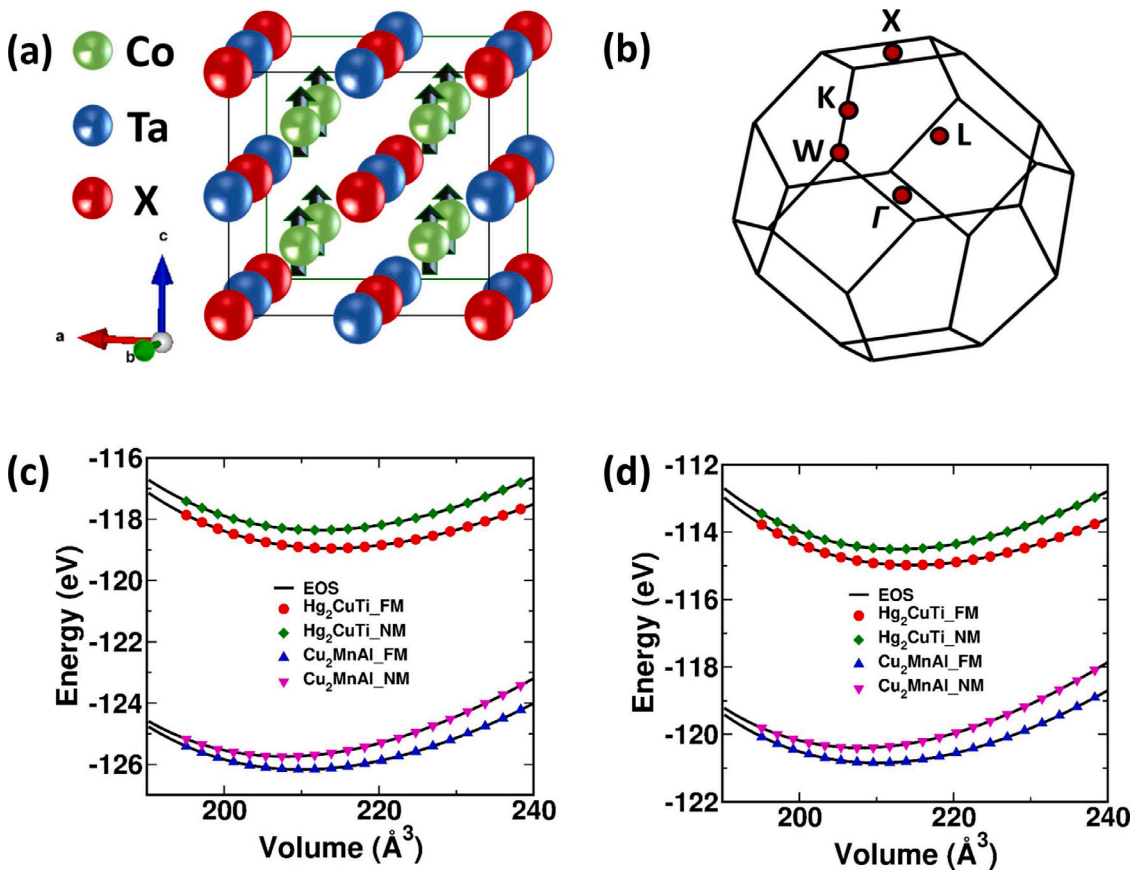

Fig. 1. (a) The cubic L21 crystal structure of Co_2TaX (X = Al, Ga). Here Co, Ta and X occupy (1/4, 1/4, 1/4), (1/2, 1/2, 1/2) and (0, 0, 0) respectively. (b) The first bulk Brillouin zone with high symmetry points marked. The Birch–Murnaghan EOS fit to the Energy–Volume curves for Co_2TaAl and Co_2TaGa in (c) and (d) respectively.

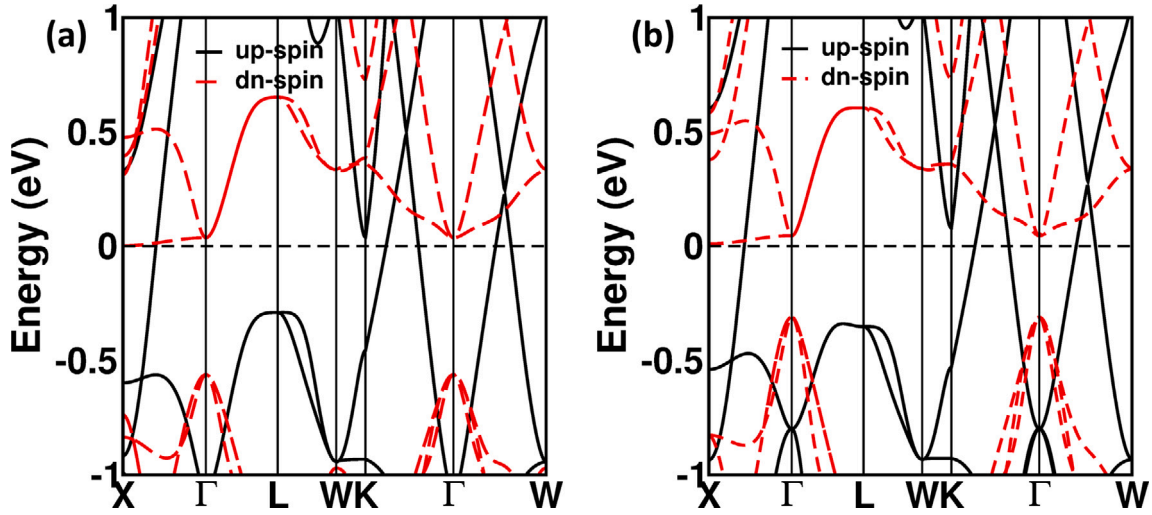

Fig. 2. The majority and minority band structures for (a) Co_2TaAl and (b) Co_2TaGa compounds. The majority and minority spin channels are respectively shown in black and dashed red colors.

Table 2
Magnetic moment given in Bohr magneton (μ_B) for the individual atoms of Co_2TaX (X = Al, Ga) in ferromagnetic (FM) configuration. The Curie temperatures from MFA are given in K.

	Co	Ta	Al/Ga	Total/cell(theoretical)	T_C(MFA)	T_C(expt)
Co_2TaAl	1.011	−0.040	0.009	1.992	560.7	260[31]
Co_2TaGa	1.013	−0.058	0.008	1.976	556.3	–

spin channel for both compounds is conducting, as indicated by the crossing of bands at Fermi level E_F, whereas minority spin channel is semiconducting, as evidenced by the presence of a finite gap at E_F for both compounds. Hence, the compounds under investigation are found to be half-metallic in nature. Magnetic Heusler compounds have always been recognized to have intriguing features due to their band structure, making them a promising class of materials. The crystal structure without magnetization has three mirror surfaces at $k_x = 0$, $k_y = 0$, and $k_z = 0$, according to the electrical properties of the

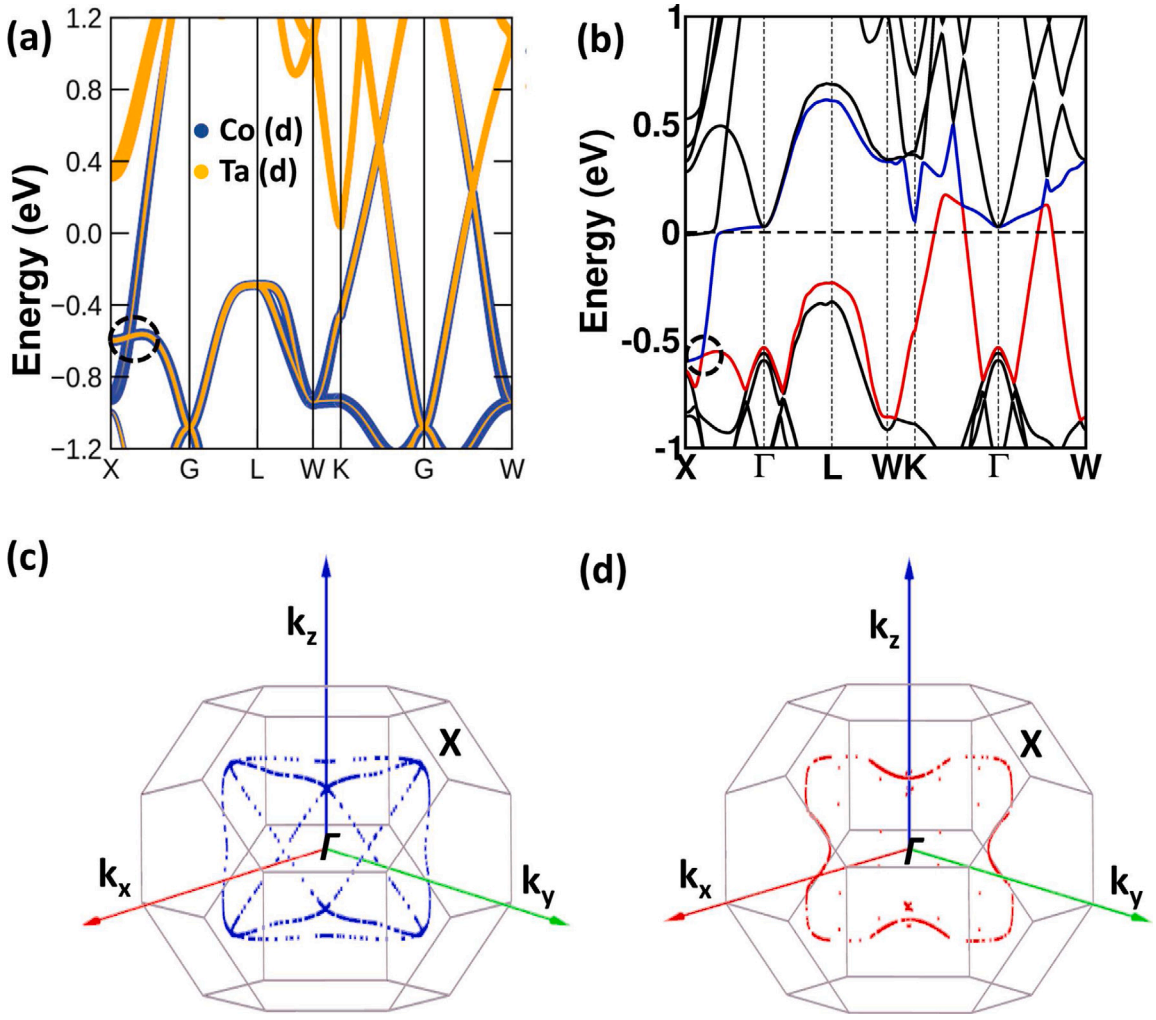

Fig. 3. (a) The majority spin band structure of Co_2TaAl with d orbital contribution of Co and Ta. (b) The band structure of Co_2TaAl with the inclusion of SOC. Nodal line behavior in Co_2TaAl w/o SOC and with SOC cases in (c) and (d). The circles in (a) and (b) represent the nodal line along Γ-X direction.

current series. The inclusion of SOC disrupts the mirror symmetries in the $k_x = 0$ and $k_y = 0$ planes by magnetization along the (001) direction. Depending on the magnetization orientation, the symmetries are disrupted in various ways. Only M_z mirror symmetry and C_4z rotational symmetry are preserved in these compounds.

For spintronic applications, the degree of spin polarization (P%) must be 100%, as measured by the spin-up and spin-down density of states at Fermi level E_F. If the density of states in the majority and minority spin channels at Fermi level E_F are $N\uparrow$ and $N\downarrow$, then the degree of spin polarization (P%) can be calculated using the equation:

$$P\% = \frac{N\uparrow(E_F) - N\downarrow(E_F)}{N\uparrow(E_F) + N\downarrow(E_F)} \times 100 \tag{3}$$

As there are no density of states $N\downarrow$ in the minority spin channel at E_F, the percentage of spin polarization (P%) for both compounds Co_2TaX (X = Al, Ga) is found to be 100% indicating that these compounds have profound spintronic applications.

3.2. Anomalous Hall and Nernst effects

The non-trivial topological features can be explained by the significant band crossings near the Fermi level E_F. The band structures of Co_2TaX (X = Al, Ga) for the majority spin scenario are shown in Fig. 3(a) and Fig. 4(a), respectively. The band crossings along the Γ-X, direction in both the compounds are marked. These nontrivial band crossings result in nodal lines in both compounds, as seen in blue lines from Fig. 3(c) and Fig. 4(c) respectively. These nontrivial band crossings in both compounds are in fact due to the character mixing of Co-*d* and Ta-*d* orbitals along Γ-X direction which are shown by a black circle in Fig. 3(a) and Fig. 4(a) respectively. Both compounds contain spatial inversion symmetry as well as nine mirror symmetries because they are cubic with space group 225. The band structures of both the compounds are depicted in Fig. 3(b) and Fig. 4(b) with the inclusion of SOC. The nodal lines along the mirror plane $M_z(k_z = 0)$ are only protected in both compounds since the magnetization is found to be along the (001) direction in both the compounds, and the nodal lines are gapped along the other planes due to broken mirror symmetry in these directions which can be seen from red lines from Fig. 3(d) and Fig. 4(d) respectively. We have concentrated on AHC in the next section since it is well known that materials with the nodal line behavior possess high AHC values.

A key band structure attribute of a solid is the Berry curvature $\Omega_{ij,n}(k)$, determining the material's topological properties [53], which is nothing more than the local gauge field associated with the Berry phase of the band structure. The Berry curvature $\Omega_{ij,n}(k)$ owing to entangled electronic Bloch bands with spin–orbit coupling inclusion when time reversal or inversion symmetry gets disrupted due to magnetization [54,55], can be written as follows [16]:

$$\Omega_{ij,n}(k) = \sum_{n\neq m} \frac{\langle n \mid \frac{\partial H}{\partial K_i} \mid m\rangle\langle m \mid \frac{\partial H}{\partial K_j} \mid n\rangle - (i \leftrightarrow j)}{(\epsilon_n - \epsilon_m)^2} \tag{4}$$

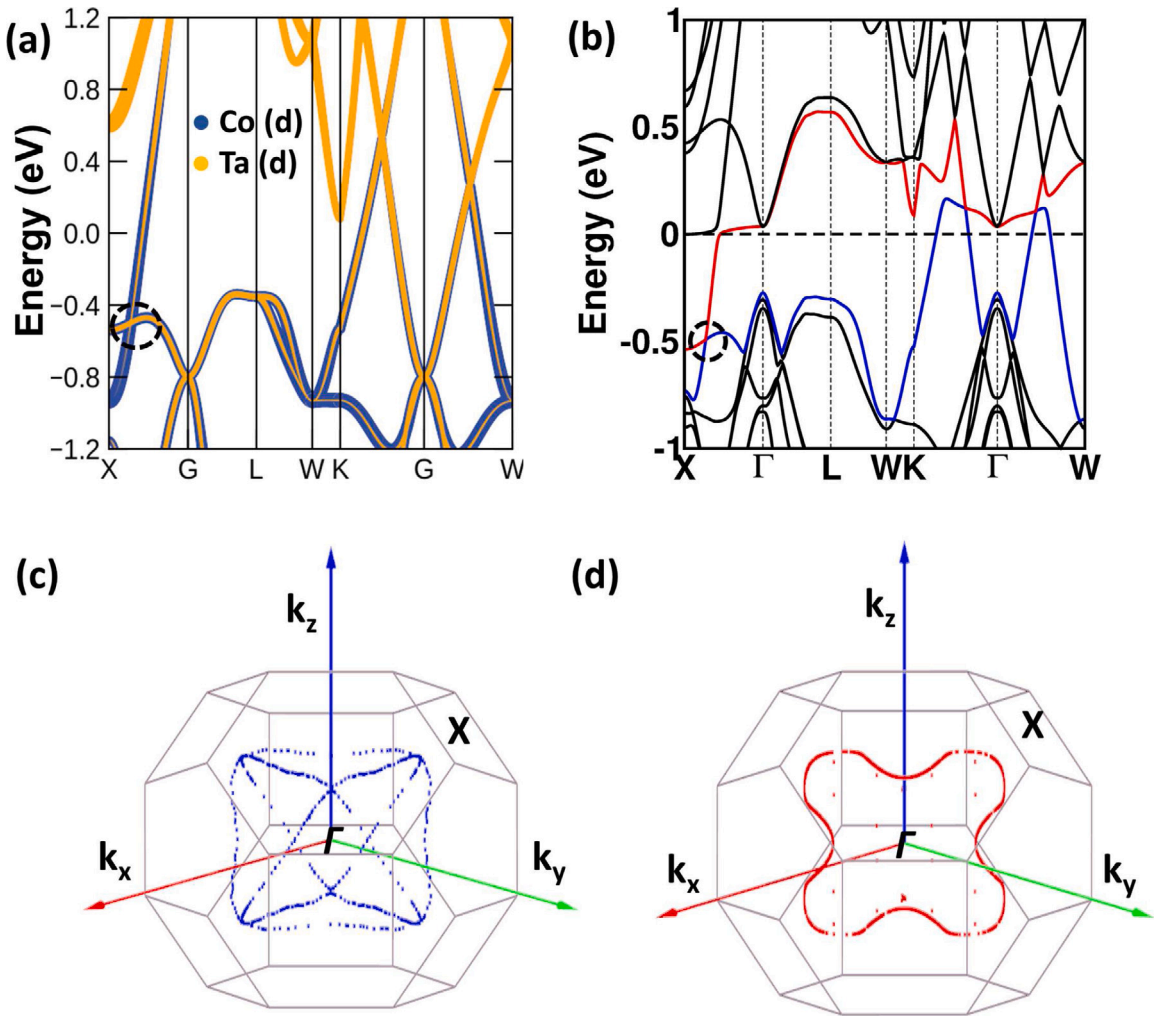

Fig. 4. (a) a) The majority spin band structure of Co_2TaGa with d orbital contribution of Co and Ta. (b) The band structure of Co_2TaGa with the inclusion of SOC. Nodal line behavior in Co_2TaGa w/o SOC and with SOC cases in (c) and (d). The circles in (a) and (b) represent the nodal line along Γ-X direction.

The eigenstates of the tight-binding Hamiltonian H derived from the wannier90 code are n and m, and their respective energies are ϵ_n and ϵ_m. AHE is a significant electronic transport phenomenon in ferromagnetic materials that describes the generation of transverse voltage perpendicular to electric current [56]. The anomalous electron velocity generated by spin–orbit coupling and magnetic field disruption causes AHE [57]. Berry curvature $\Omega_{ij,n}(k)$ across all occupied electronic bands in the Brillouin zone below the Fermi level E_F [53] is the intrinsic AHE. Hence, the Berry curvature $\Omega_{ij,n}(k)$ driven AHE σ_{xy}[58], can be represented as follows:

$$\sigma_{xy} = \frac{-e^2}{\hbar}\sum_n \int \frac{d^3k}{(2\pi)^3} f(k)\Omega_{ij,n}(k) \tag{5}$$

where e, $\hbar$, $f(k)$ denotes the charge of an electron, reduced Planck's constant, and the Fermi–Dirac distribution function. Y. Ji et al. [59], in their article pointed out that the key mechanism for anomalous velocity is mixing of d_{xz}, d_{yz} or d_{xy}, $d_{x^2-y^2}$ orbitals due to SOC. So, the AHC may be caused by not only due to SOC strength but also may be due to atomic orbitals interactions. AHC may also depend on electronic band structure and wave functions, and large AHC may be due to nodal lines. One may figure out the significant AHC values at proper places in band structure along particular paths. The Anomalous Nernst effect is the thermoelectric analog of the ANE. It is a type of magneto-thermoelectric effect found in spin-caloritronics. The development of a transverse electric field as a result of the material's magnetization generated by a longitudinal temperature gradient, rather than by an externally provided magnetic field, is characterized as ANE [60]. Non-zero Berry curvature $\Omega_{ij,n}(k)$, which operates as a fictitious magnetic field [56], causes both AHC and ANE. Initially, ANE was considered to be proportional to magnetization, but it was recently proposed that it comes from Berry curvature $\Omega_{ij,n}(k)$ of all bands near Fermi level E_F[53]. As a result, the anomalous off-diagonal thermoelectric coefficient, known as the Anomalous Nernst Conductivity (ANC) α_{xy}[58], can be written as:

$$\alpha_{xy}(T,\mu) = -\frac{1}{e}\sum_n \int d\epsilon \frac{\partial f(\epsilon-\mu,T)}{\partial \epsilon}.\frac{\epsilon-\mu}{T}\sigma_{xy}(\epsilon) \tag{6}$$

where μ is the chemical potential. The above equation [58] for near zero temperature becomes,

$$\left.\frac{\alpha_{xy}}{T}\right|_{T\to 0} = -\frac{\pi^2}{3}\frac{k_B^2}{|e|}\frac{d\sigma_{xy}}{d\mu} \tag{7}$$

where k_B is Boltzmann's constant. Designing a large Berry curvature yields large ANC and nodal points, nodal lines in momentum space are responsible for enhancement in Berry curvature. Therefore, a large ANE is exhibited by ferromagnets due to the enhancement of the Berry curvature which is beyond the conventional linear scaling law with magnetization [61]. Fig. 5(a,e) and Fig. 5(d,h) show the band structure and Berry curvature $\Omega_{ij,n}(k)$ with SOC along the high symmetry path for Co_2TaAl and Co_2TaGa compounds, respectively. As can be observed in Fig. 5(a and e), the derived DFT band structure from VASP is quite similar to the wannier90 band structure for both compounds. The

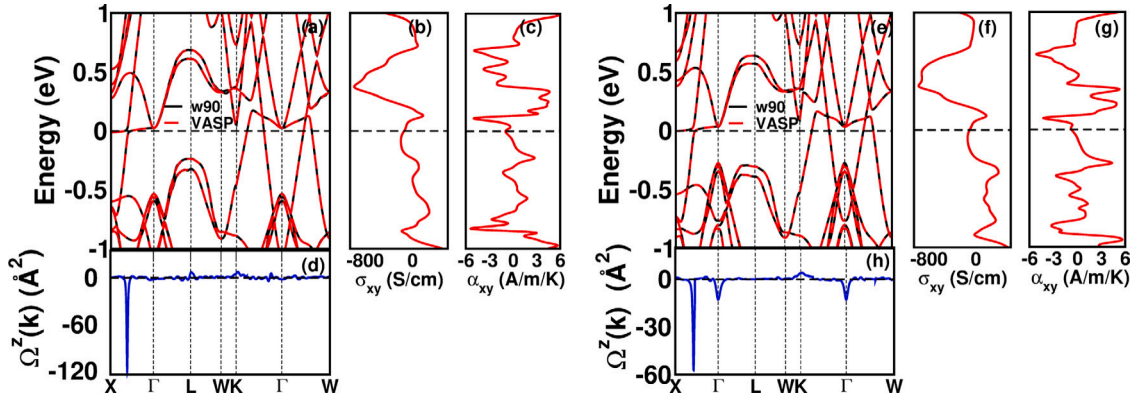

Fig. 5. (a,e) The band structure with the inclusion of spin–orbit coupling, (b,f) Anomalous Hall Conductivity σ_{xy}, (c,g) Anomalous Nernst Conductivity α and (d,h) Berry curvature along the high symmetry path for Co_2TaAl and Co_2TaGa compounds. The band structures using wannier90 and VASP are shown in solid black and dashed red lines respectively.

energy gaps created by spin–orbit coupling contribute only a small amount to the denominator of Eq. (4), resulting in a non-vanishing $\Omega_{ij,n}(k)$. The Berry curvature of Co_2TaAl and Co_2TaGa compounds has peaks and valleys, as seen from Fig. 5(d and h). From Fig. 5(d), it is seen that the Berry curvature $\Omega_{ij,n}(k)$ is having a large prominent peak along $\Gamma - X$ direction, and other significant peaks around L and K directions for Co_2TaAl. Similarly, Fig. 5(h), one can observe a huge peak along $\Gamma - X$ direction, and other significant peaks around $\Gamma - L$ and $\Gamma - K$ directions for Co_2TaGa. From the band structure with spin–orbit interaction shown in Fig. 5(a,e), avoided crossings are discovered at the chemical potential, which may also contribute to the non-vanishing huge peak in $\Omega_{ij,n}(k)$ along the $\Gamma - X$ direction and, as a result, give rise to the AHC and ANC in these compounds. The AHC σ_{xy} (S/cm) and ANC α_{xy} ($Am^{-1}K^{-1}$) are plotted as a function of $E - E_F$ (eV) as shown Fig. 5(b,c) and Fig. 5(f,g) respectively for Co_2TaAl and Co_2TaGa. The maximum values of AHC and ANC are found within the energy range of ±300 meV near the Fermi level E_F. The maximum obtained value of AHC is −602.8 S/cm at 300 meV and ANC at room temperature is −4.989 $Am^{-1}K^{-1}$ at 108 meV for Co_2TaAl from Fig. 5(b and c). Similarly, for Co_2TaGa across the ±300 meV range above and below Fermi level E_F, the maximum value of AHC is −593.8 S/cm at 300 meV, and ANC at ambient temperature is 4.934 $Am^{-1}K^{-1}$ at 218.4 meV, as shown in Fig. 5(f and g). The obtained AHC values for both compounds Co_2TaX (X = Al, Ga) are comparable to the AHC values of other Heusler alloys.

3.3. Magnetic exchange interactions

The Heisenberg magnetic exchange coupling J_{ij} between atoms is explored in Co_2TaX (X = Al, Ga) compounds to investigate the ground state magnetic configuration. The nature of magnetism exhibited by the system is given by the exchange coupling constant J_{ij}, whose value being positive and negative depicts the FM and AFM connections between atoms. The classical Heisenberg Hamiltonian gives the estimation of the exchange coupling amid the atoms by [62,63]

$$H_{eff} = -\sum_{\chi\psi}\sum_{ij} J_{ij}^{\chi\psi} e_i^{\chi} e_j^{\psi} \tag{8}$$

where χ and ψ are individual sublattices, i and j represent atomic locations, and e_i^{χ}, e_j^{ψ} represent the magnetic moment of i, j atoms in sublattices χ and ψ respectively. The T_C is calculated as follows:

$$T_C = \frac{2}{3k_B} J_{max} \tag{9}$$

With the greatest eigenvalue of the effective exchange coupling constant J_{eff} is J_{max}, which is represented as:

$$J_{eff}^{\chi\psi} = \sum_{j\neq 0} J_{0j}^{\chi\psi} \tag{10}$$

where j represents all atomic positions in the sublattice ψ in the sphere of radius $4.5a$, where a is the optimal lattice constant of Co_2TaX (X = Al, Ga), and 0 indicates a specific atomic position within the χ-sublattice.

The magnetic exchange coupling for compounds Co_2TaX (X = Al, Ga) is given by J_{ij} between sites i and j as a function of R_{ij}, as shown in the Fig. 6(a,b), where the nearest neighbor distance is R_{ij} and optimized lattice constant is a. Here the interactions Co_1-Co_2 and Co_1-Co_1/Co_2-Co_2 have prominent contribution to the exchange coupling J_{ij} in both compounds as shown Fig. 6(a,b). The other interactions such as Co–Ta, Co–Al, Co-Ga, Ta–Ta, Ta–Al, Ta–Ga, Al–Al and Al–Ga are not contributing. Coming to Co_2TaAl compound, the initial four nearest-neighbor interactions are positive for Co_1-Co_2 while the fifth, sixth and seventh ones are negative as shown in Fig. 6(a) and first two nearest-neighbor interactions are negative for Co_1-Co_1/Co_2-Co_2 interaction while the next four interactions are positive, again seventh and eighth interactions are negative. The positive and negative oscillatory behavior of these Co_1-Co_2 and Co_1-Co_1/Co_2-Co_2 interactions indicate the RKKY-type interaction in Co_2TaAl. Though the negative interactions are observed, still the positive interactions dominate over them. Hence, the compound is found to be ferromagnetic nature. The same trend is observed with Co_1-Co_2 and Co_1-Co_1/Co_2-Co_2 interactions in Co_2TaGa as shown in Fig. 6(b). Using the Heisenberg exchange interactions, the estimated T_C of Co_2TaAl and Co_2TaGa compounds from mean-field approximation are 560.7 K and 556.3 K respectively which are tabulated in Table 2 along with the available experimental T_C[31] values. From Table 2, it is found that the T_C of Co_2TaAl from MFA is higher than that of the experimental value [64], which is expected as magnetic fluctuations get neglected at longer wavelengths.

3.4. Mechanical and dynamical stability

The mechanical stability of Co_2TaX (X = Al, Ga) compounds are ensured by computing the elastic constants C_{ij}. The three elastic constants of examined cubic compounds C_{11}, C_{12} and C_{44}, as well as their derived elastic properties such as Young's modulus (E), Bulk modulus (B), average shear modulus (G) and Poisson's ratio, etc., obtained from Voigt–Reuss–Hill approximation [65] are shown in Table 3. The Born mechanical stability criteria [66] ensures the mechanical stability of the compounds under investigation i.e. $C_{11}>0$, $C_{44}>0$, $C_{11}>C_{12}$ and $C_{11}+2C_{12}>0$. The relation among the elastic constant C_{ij} and other parameters are found elsewhere [48,67,68]. The Young's modulus (E) in general indicates the rigidness of a material, and the E values for Co_2TaX (X = Al, Ga) are 262.47 GPa and 248.78 GPa, respectively, showing that Co_2TaAl is more rigid than Co_2TaGa. As can be observed from the data in Table 3, the higher the shear modulus (G), the higher the hardness, which is higher in Co_2TaAl than in Co_2TaGa.

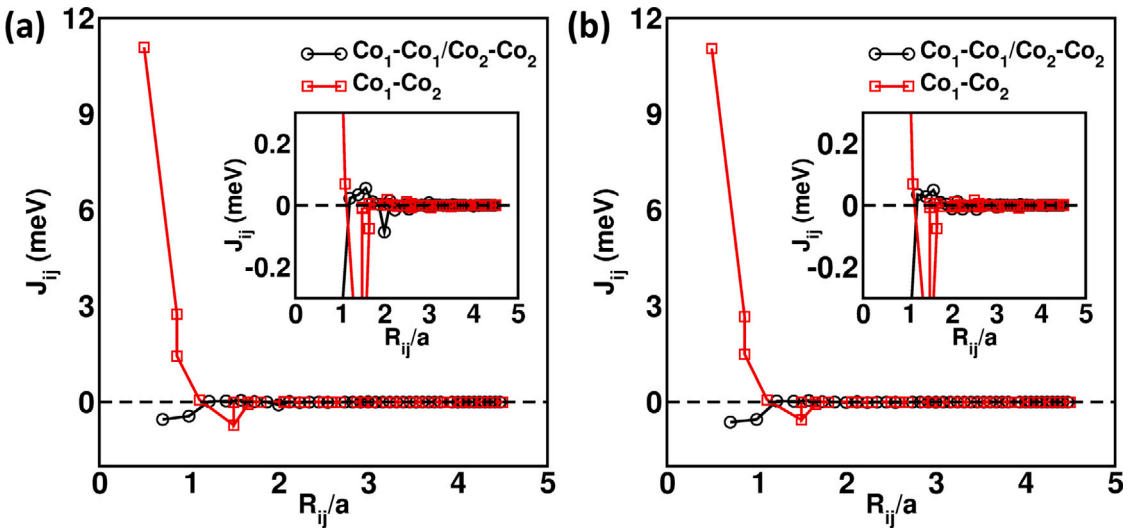

Fig. 6. The Heisenberg exchange interactions for Co_2TaAl in (a) and Co_2TaGa in (b). The interactions between Co_1-Co_1/Co_2-Co_2 and Co_1-Co_2 are shown here and other interactions are omitted as they are negligible.

Table 3
Co_2TaX (X = Al, Ga) single crystalline elastic constants at ambient pressure in GPa, where E is Young's modulus in GPa, σ is Poisson's ratio, A is anisotropy factor, P_C = Cauchy's pressure (C_{12}–C_{44}) in GPa, G/B = Pugh's ratio, V_l, V_t and V_m are longitudinal, transverse and mean sound velocities in km/s and Θ_D is Debye temperature in *Kelvin*.

Parameters	Co_2TaAl	Co_2TaGa
C_{11}	305.83	296.52
C_{12}	148.23	167.32
C_{44}	121.93	124.04
Anisotropy factor *A*	1.54	1.92
G_V	104.68	100.26
G_R	100.03	90.67
B	200.76	210.38
G	102.35	95.47
E	262.47	248.78
B/G	1.96	2.20
Poisson's ratio σ	0.28	0.30
P_C	26.3	43.28
G/B	0.50	0.45
V_l	5.72	5.38
V_t	3.15	2.86
V_m	3.51	3.19
Θ_D	443.48	403.77

As the bulk modulus (B) value for Co_2TaGa is higher compared to that of Co_2TaAl, it is very hard to be compressed. The Anisotropy factor (A) is used to explore microcracks in materials and the compounds under study are anisotropic in nature as their A value is different from unity. The Cauchy's pressure (P_C), Pugh's ratio (G/B) and Poisson's ratio (σ) define the ductility and brittleness of the solids and if G/B< 0.57, $C_{12} - C_{44}$>0 and σ>0.26, then the solid is said to be ductile and here both the compounds under study satisfy these conditions indicating that they are ductile in nature. The most fundamental parameter of a solid is the Debye temperature (Θ_D) which differentiates between low and high temperature regions of a solid. The obtained Debye temperature (Θ_D) values are 443.4 *K* and 403.7 *K* respectively for Co_2TaAl and Co_2TaGa as given in Table 3.

The dynamical stability of the investigated compounds is ensured by the lack of imaginary frequencies in the phonon dispersion plots and phonon density of states for both compounds as shown in Fig. 7(a,b). In Co_2TaAl, there is a very narrow gap between the optical and acoustic phonon modes, but in Co_2TaGa, they overlap. The difference in atomic masses between Co, Ta, Al, and Ga is well known. Co, Ta, and Ga have similar atomic masses, which causes coupled phonon dispersions, whereas Al has a much lower atomic mass, which causes phonon separation. Furthermore, the phonon density of states well explains phonon dynamics in both the compounds. The atoms Co, Ta, Al and Ga atoms contribute to low, mid, and high frequencies as seen from Fig. 7(a,b). The phonon density of states that separates the acoustic and optical regions is discovered to have a finite gap. It is observed that the slope of phonon levels at the Γ point mimics a Dirac shape, indicating the heat transmission capabilities at low temperatures for both the compounds. Despite their static, dynamic, and atomic similarities, Co_2TaAl and Co_2TaGa compounds display different thermal and optical behavior due to the two different atoms, Al and Ga, in their structure. The longitudinal phonon energy level gradients in the range of 0 to 200 cm^{-1}, indicates that Co_2TaGa is an outstanding thermal and optical energy transducer.

3.5. Magneto-optical Kerr effect (MOKE)

MOKE (magneto-optical Kerr effect) is a widely used technique for determining magnetic properties in materials. Quantum confinement effects [69], Kerr rotation oscillations with magnetic layer thickness [70], and strong correlations between MOKE and magnetic anisotropies [71] are just a few of the recent exciting MOKE discoveries. MOKE is crucial in terms of both technology and science since it provides deeper information on the electronic structure of magnetic materials. One among in its recent usagees is the readout processes in magneto-optical (MO) storage systems, which paved way for a lot of research in identifying materials with large Kerr rotation angles [72]. The MOKE phenomenon arises because of the co-existence of spin polarization and spin–orbit coupling [73]. The production of prominent peaks in the MOKE spectrum are linked to interband transitions [74] and half-metallic ferromagnetism with spin–orbit coupling [75], and free charge carrier plasma resonances [76]. Therefore, a theoretical analysis of MOKE must undoubtedly consider both spin–orbit coupling and spin polarization. Also it is essential that the Kerr rotation estimation requires correct values of both the dispersive and absorptive sections of the off-diagonal elements of the conductivity tensor. As both spin–orbit coupling and exchange splitting create tiny changes in the band structure, these values are difficult to calculate. MOKE is based on the conversion of linearly polarized light into elliptically polarized light with an angle (relative to the incident polarization plane) which is reflected from a ferromagnetic material. The polar Kerr effect is examined when both the incoming wave vector and the magnetization vector are perpendicular to the surface. The polar Kerr angle (θ_K) is

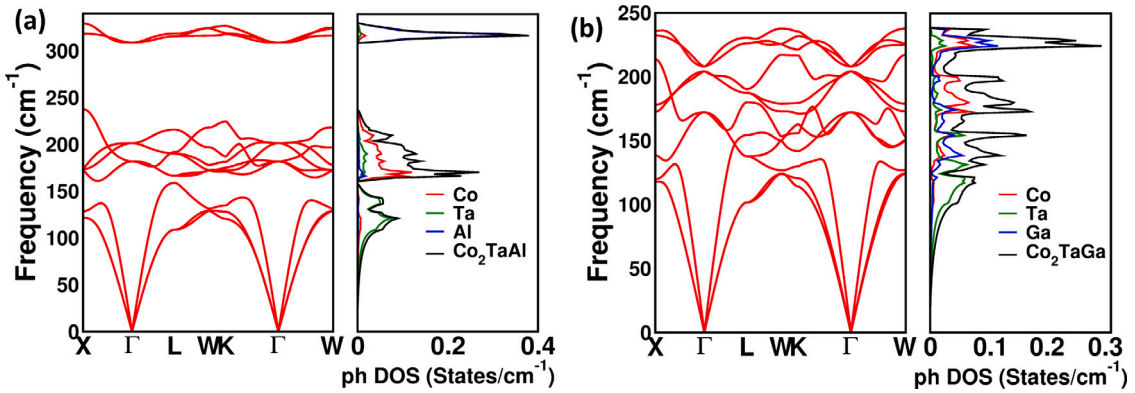

Fig. 7. The phonon dispersion plots for (a) Co_2TaAl and (b) Co_2TaGa compounds.

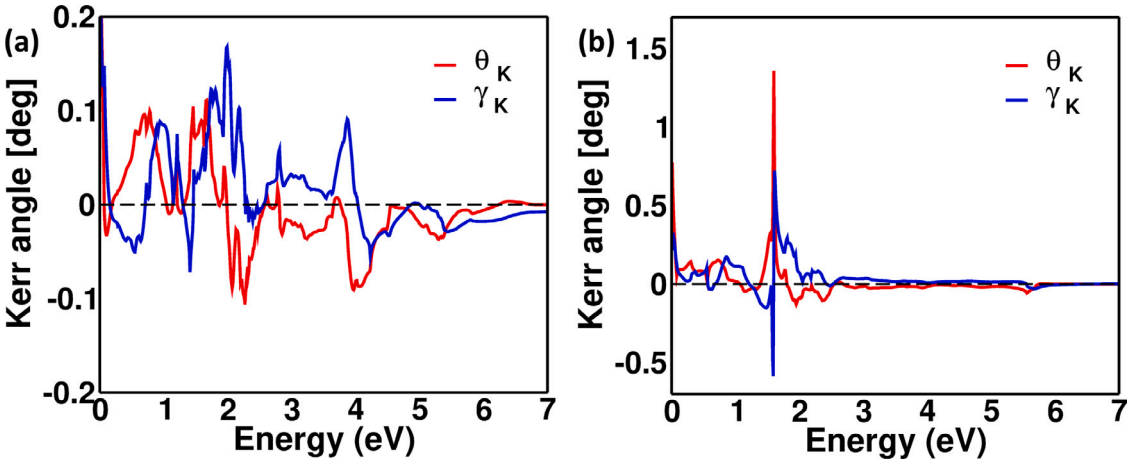

Fig. 8. The Kerr angle (θ_K) and ellipticity (γ_K) calculated at normal incidence versus optical energy for (a) Co_2TaAl and (b) Co_2TaGa compounds.

a complicated angle that may be calculated using the macroscopic conductivity tensor as given by:

$$\phi_K = \theta_K + i\gamma_K = \frac{-\sigma_{xy}}{\sigma_{xx}\sqrt{1 + i(\frac{4\pi}{\omega})\sigma_{xx}}} \tag{11}$$

where θ_K (real part) is the Kerr-rotation angle, γ_K (imaginary part) is the Kerr ellipticity, ω is the transition energy and σ_{xx}, σ_{xy} are the optical conductivity tensor components. As these compounds have 100% spin polarization and are half-metallic in nature, the magnetic component of light is expected to interact with the magnetic moment whenever the electromagnetic spectrum of light falls on their surface. The reflection of photons from their surface causes the polarization of light to be seen. Looking at the case of Co_2TaAl from Fig. 8(a), considerable changes in the Kerr angle θ_K and ellipticity γ_K are observed. The Kerr spectra followed by positive and negative peaks corresponds to the clockwise and counter-clockwise polarization of light. At the verge of visible region, a significant peak is found with a value of 0.11° at 1.6 eV. As the energy of the reflected photon increases, same as its polarization, the electric field of reflected light changes its rotation from clockwise to counterclockwise. As a result, there is a shift in the nature of its polarization and magnitude.

On the contrary, in the case of Co_2TaGa from Fig. 8(b), it is found that a singular peak with a value of 1.35° is observed at 1.6 eV. The rotation of the electric field is more in the clockwise direction, as seen by the peak value of γ_K that corresponds to the rotation. Hence, the sharp positive peak indicates that the compound Co_2TaGa to be a good polarized material with a large Kerr angle of 1.35°. The nature of the material, the saturation magnetization of the surface domains, the incident wavelength, and the incidence angle influences the size of the Kerr effect. The maximal value of Kerr angle is taken in a range from 1 to 5 eV and given in Table 4. As a result, any magnetic substance with a sufficiently flat surface can be subjected to the Kerr effect which will have profound applications in the magneto-optic industry.

Table 4
Calculated values of polar Kerr angle at normal incidence (θ_K) in degree (°) with maximal values taken in a range from 1 eV to 5 eV.

Compound	$\theta_K(max)$
Co_2TaAl	0.11
Co_2TaGa	1.35

4. Conclusion

The Co_2TaX (X = Al, Ga) compounds are discovered to be half-metals as they obey the Slater–Pauling rule with 100% spin polarization. In the majority spin channel, both compounds have nodal lines, but when SOC is added, they become Weyl nodes. Within the range of ±300 meV around E_F, the Berry curvature induced anomalous Hall and Nernst conductivity of Co_2TaX (X = Al, Ga) compounds are probed in. The maximum value of AHC is −602.8 S/cm at 300 meV and ANC at room temperature is −4.989 $Am^{-1}K^{-1}$ at 108 meV for Co_2TaAl compound, while for Co_2TaGa the maximum value of AHC is −593.8 S/cm at 300 meV and ANC at room temperature is 4.934 $Am^{-1}K^{-1}$ at 218.4 meV. The Heisenberg magnetic exchange interactions are studied and their estimated Curie temperatures (T_C) within the mean-field approximation are 560.7 K and 556.3 K respectively. Born

stability criteria and phonon dispersion plots are used to confirm the mechanical and dynamical stability of Co_2TaX (X = Al, Ga) compounds. In addition, magneto-optical response is also examined, and the polar Kerr rotation angles were found to be 0.11° and 1.35° for Co_2TaAl and Co_2TaGa at normal incidence. As a result of this research, accurate property engineering in real-world applications may be possible.

CRediT authorship contribution statement

P. Rambabu: Software, Methodology, Validation, Visualization, Writing – review & editing. **Anusree C.V.:** Software, Methodology, Validation, Visualization, Writing – review & editing. **M. Manivel Raja:** Conceptualization, Methodology, Validation, Visualization, Writing – review & editing. **V. Kanchana:** Conceptualization, Software, Methodology, Validation, Visualization, Project administration, Writing – review & editing.

Declaration of competing interest

The authors declare that they have no known competing financial interests or personal relationships that could have appeared to influence the work reported in this paper.

Data availability

Data will be made available on request.

Acknowledgment

The authors PR and VK would like to thank IIT Hyderabad and National PARAM Supercomputing Facility (NPSF) and Centre for Development of Advanced Computing (C-DAC), Pune for computational facility and PR acknowledges Guru Ghasidas Vishwavidyalaya, Bilaspur, C.G. for sponsoring Ph.D. Authors would like to acknowledge Alexander N. Rudenko for fruitful discussions and critical reading of the manuscript. A C.V and VK acknowledges DRDO project with reference number (ERIP/ER/201701001/M/01/1711).

References

[1] V.G. de Paula, M.S. Reis, Chem. Mater. 33 (2021) 5483–5495, http://dx.doi.org/10.1021/acs.chemmater.1c01012.
[2] A.Q. Seh, D.C. Gupta, Int. J. Energy Res. 43 (2019) 8864–8877, http://dx.doi.org/10.1002/er.4853.
[3] T. Eto, X. Xu, T. Ito, F. Honda, D. Li, G. Oomi, F. Nakamura, H. Masumoto, R. Kainuma, T. Kanomata, J. Alloys Compd. 871 (2021) 159480, http://dx.doi.org/10.1016/j.jallcom.2021.159480.
[4] D.J. Mokhtari, I. Jum'h, H. Baaziz, Z. Charifi, T. Ghellab, A. Telfah, R. Hergenröder, Phil. Mag. 100 (2020) 1636–1661, http://dx.doi.org/10.1080/14786435.2020.1731926.
[5] Y. Lakred, S. Bahlouli, M. Elchikh, Eur. Phys. J. B 94 (2021) 1–10, http://dx.doi.org/10.1140/epjb/s10051-021-00141-8.
[6] M.J. Winiarski, G. Kuderowicz, K. Górnicka, L.S. Litzbarski, K. Stolecka, B. Wiendlocha, R.J. Cava, T. Klimczuk, Phys. Rev. B 103 (2021) 214501, http://dx.doi.org/10.1103/PhysRevB.103.214501.
[7] E.M. Carnicom, W. Xie, Z. Yang, K. Górnicka, T. Kong, T. Klimczuk, R.J. Cava, Chem. Mater. 31 (2019) 2164–2173, http://dx.doi.org/10.1021/acs.chemmater.9b00258.
[8] T. Kubota, Z. Wen, K. Takanashi, J. Magn. Magn. Mater. 492 (2019) 165667, http://dx.doi.org/10.1016/j.jmmm.2019.165667.
[9] J. Zhang, T. Phung, A. Pushp, Y. Ferrante, J. Jeong, C. Rettner, B.P. Hughes, S.-H. Yang, Y. Jiang, S.S.P. Parkin, Appl. Phys. Lett. 110 (2017) 172403, http://dx.doi.org/10.1063/1.4981388.
[10] J. Han, Y. Feng, K. Yao, G.Y. Gao, Appl. Phys. Lett. 111 (2017) 132402, http://dx.doi.org/10.1063/1.4999288.
[11] K. Seema, N.M. Umran, K. Ranjan, J. Supercond. Nov. Magn. 29 (2016) 401–408, http://dx.doi.org/10.1002/er.4853.
[12] J. Noky, Y. Zhang, J. Gooth, C. Felser, Y. Sun, Npj Comput Mater 6 (2020) 77, http://dx.doi.org/10.1038/s41524-020-0342-5.
[13] S.K. Lyo, T. Holstein, Phys. Rev. Lett. 29 (1972) 423–425, http://dx.doi.org/10.1103/PhysRevLett.29.423.
[14] L. Berger, Phys. Rev. B 5 (1972) 1862–1870, http://dx.doi.org/10.1103/PhysRevB.5.1862.
[15] P. Leroux-Hugon, A. Ghazali, J. Phys. C 5 (1972) 1072–1081, http://dx.doi.org/10.1088/0022-3719/5/10/012.
[16] D. Xiao, M.-C. Chang, Q. Niu, Rev. Modern Phys. 82 (2010) 1959–2007, http://dx.doi.org/10.1103/RevModPhys.82.1959.
[17] H. Kontani, T. Tanaka, K. Yamada, Phys. Rev. B 75 (2007) 184416, http://dx.doi.org/10.1103/PhysRevB.75.184416.
[18] Y. Yao, L. Kleinman, A.H. MacDonald, J. Sinova, T. Jungwirth, D.-s. Wang, E. Wang, Q. Niu, Phys. Rev. Lett. 92 (2004) 037204, http://dx.doi.org/10.1103/PhysRevLett.92.037204.
[19] N. Nagaosa, J. Sinova, S. Onoda, A.H. MacDonald, N.P. Ong, Rev. Modern Phys. 82 (2010) 1539–1592, http://dx.doi.org/10.1103/RevModPhys.82.1539.
[20] J. Kübler, C. Felser, Phys. Rev. B 85 (2012) 012405, http://dx.doi.org/10.1103/PhysRevB.85.012405.
[21] R. Karplus, J.M. Luttinger, Phys. Rev. 95 (1954) 1154–1160, http://dx.doi.org/10.1103/PhysRev.95.1154.
[22] P. Li, J. Koo, W. Ning, J. Li, L. Miao, L. Min, Y. Zhu, Y. Wang, N. Alem, C.-X. Liu, et al., Nature Commun. 11 (2020) 1–8, http://dx.doi.org/10.1038/s41467-020-17174-9.
[23] C. Fowley, K. Rode, Y.-C. Lau, N. Thiyagarajah, D. Betto, K. Borisov, G. Atcheson, E. Kampert, Z. Wang, Y. Yuan, S. Zhou, J. Lindner, P. Stamenov, J.M.D. Coey, A.M. Deac, Phys. Rev. B 98 (2018) 220406, http://dx.doi.org/10.1103/PhysRevB.98.220406.
[24] D. Dyck, A. Becker, J. Koo, T. Matalla-Wagner, J. Krieft, G. Reiss, Physica Status Solidi (B) 258 (2021) 2000067.
[25] B. Ernst, R. Sahoo, Y. Sun, J. Nayak, L. Müchler, A.K. Nayak, N. Kumar, J. Gayles, A. Markou, G.H. Fecher, C. Felser, Phys. Rev. B 100 (2019) 054445, http://dx.doi.org/10.1103/PhysRevB.100.054445.
[26] G.K. Shukla, J. Sau, N. Shahi, A.K. Singh, M. Kumar, S. Singh, Phys. Rev. B 104 (2021) 195108, http://dx.doi.org/10.1103/PhysRevB.104.195108.
[27] S.A. Khandy, D.C. Gupta, Semicond. Sci. Technol. 32 (2017) 125019, http://dx.doi.org/10.1088/1361-6641/aa9785.
[28] M. Ayad, F. Belkharroubi, F. Boufadi, M. Khorsi, M. Zoubir, M. Ameri, I. Ameri, Y. Al-Douri, K. Bidai, D. Bensaid, Indian J. Phys. 94 (2020) 767–777, http://dx.doi.org/10.1007/s12648-019-01518-3.
[29] R. Mohebbi, A. Boochani, S. Rezaee, Int. Nano Lett. 10 (2020) 81–88, http://dx.doi.org/10.1007/s40089-020-00296-9.
[30] Y. Miuraa, M. Shirai, K. Nagao, J. Appl. Phys. 99 (2006) 08J112, http://dx.doi.org/10.1063/1.2176907.
[31] K. Buschow, P. van Engen, J. Magn. Magn. Mater. 25 (1981) 90–96, http://dx.doi.org/10.1016/0304-8853(81)90151-7.
[32] A. Carbonari, R. Saxena, W. Pendl, J. Mestnik Filho, R. Attili, M. Olzon-Dionysio, S. de Souza, J. Magn. Magn. Mater. 163 (1996) 313–321, http://dx.doi.org/10.1016/S0304-8853(96)00338-1.
[33] P. van Engena, K. Buschow, R. Jongebreur, M. Erman, Appl. Phys. Lett. 42 (1983) 202, http://dx.doi.org/10.1063/1.93849.
[34] V.N. Antonov, A.N. Yaresko, A.Y. Perlov, V.V. Nemoshkalenko, P.M. Oppeneer, H. Eschrig, Low Temp. Phys. 25 (1999) 387–406, http://dx.doi.org/10.1063/1.593756.
[35] P.E. Blöchl, Phys. Rev. B 50 (1994) 17953–17979, http://dx.doi.org/10.1103/PhysRevB.50.17953.
[36] G. Kresse, J. Furthmüller, Phys. Rev. B 54 (1996) 11169–11186, http://dx.doi.org/10.1103/PhysRevB.54.11169.
[37] G. Kresse, D. Joubert, Phys. Rev. B 59 (1999) 1758–1775, http://dx.doi.org/10.1103/PhysRevB.59.1758.
[38] H.J. Monkhorst, J.D. Pack, Phys. Rev. B 13 (1976) 5188–5192, http://dx.doi.org/10.1103/PhysRevB.13.5188.
[39] J.P. Perdew, K. Burke, M. Ernzerhof, Phys. Rev. Lett. 77 (1996) 3865–3868, http://dx.doi.org/10.1103/PhysRevLett.77.3865.
[40] H. Ebert, D. Ködderitzsch, J. Minár, Rep. Progr. Phys. 74 (2011) 096501, http://dx.doi.org/10.1088/0034-4885/74/9/096501.
[41] A. Togo, I. Tanaka, Scr. Mater. 108 (2015) 1–5, http://dx.doi.org/10.1016/j.scriptamat.2015.07.021.
[42] G. Pizzi, V. Vitale, R. Arita, S. Blügel, F. Freimuth, G. Géranton, M. Gibertini, D. Gresch, C. Johnson, T. Koretsune, J. Ibañez-Azpiroz, H. Lee, J.-M. Lihm, D. Marchand, A. Marrazzo, Y. Mokrousov, J.I. Mustafa, Y. Nohara, Y. Nomura, L. Paulatto, S. Poncé, T. Ponweiser, J. Qiao, F. Thöle, S.S. Tsirkin, M. Wierzbowska, N. Marzari, D. Vanderbilt, I. Souza, A.A. Mostofi, J.R. Yates, J. Phys.: Condens. Matter 32 (2020) 165902, http://dx.doi.org/10.1088/1361-648x/ab51ff.
[43] Q. Wu, S. Zhang, H.-F. Song, M. Troyer, A.A. Soluyanov, Comput. Phys. Comm. 224 (2018) 405–416, http://dx.doi.org/10.1016/j.cpc.2017.09.033.
[44] X. Wang, J.R. Yates, I. Souza, D. Vanderbilt, Phys. Rev. B 74 (2006) 195118, http://dx.doi.org/10.1103/PhysRevB.74.195118.
[45] N. Marzari, D. Vanderbilt, Phys. Rev. B 56 (1997) 12847–12865, http://dx.doi.org/10.1103/PhysRevB.56.12847.
[46] N. Marzari, A.A. Mostofi, J.R. Yates, I. Souza, D. Vanderbilt, Rev. Modern Phys. 84 (2012) 1419–1475, http://dx.doi.org/10.1103/RevModPhys.84.1419.
[47] I. Galanakis, P.H. Dederichs, N. Papanikolaou, Phys. Rev. B 66 (2002) 174429, http://dx.doi.org/10.1103/PhysRevB.66.174429.

[48] P. Rambabu, C.V. Anusree, M.M. Raja, V. Kanchana, J. Magn. Magn. Mater. 538 (2021) 168303, http://dx.doi.org/10.1016/j.jmmm.2021.168303.
[49] L. Bing, Z. Lian, Y. Miao, et al., Appl. Phy. Lett. 116 (2020) 132404, http://dx.doi.org/10.1063/1.5144904.
[50] R. Mohankumar, S. Ramasubramanian, M. Rajagopalan, et al., J. Mater. Sci. 50 (2015) 1287–1294, http://dx.doi.org/10.1007/s10853-014-8687-0.
[51] H.P. James, C. Loach, J. Smith, et al., J. Magn. Soc. Jpn. 38 (2014) 50–55, http://dx.doi.org/10.3379/msjmag.1402R010.
[52] P. Bruski, S. Erwin, M. Ramsteiner, et al., Phys. Rev. B. 83 (2011) 140409, http://dx.doi.org/10.1103/PhysRevB.83.140409.
[53] S.N. Guin, K. Manna, J. Noky, S.J. Watzman, C. Fu, N. Kumar, W. Schnelle, C. Shekhar, Y. Sun, J. Gooth, et al., NPG Asia Mater. 11 (2019) 1–9, http://dx.doi.org/10.1038/s41427-019-0116-z.
[54] B.K. Hazra, S.N. Kaul, S. Srinath, M.M. Raja, R. Rawat, A. Lakhani, Phys. Rev. B 96 (2017) 184434, http://dx.doi.org/10.1103/PhysRevB.96.184434.
[55] E. Liu, Y. Sun, N. Kumar, L. Muechler, A. Sun, L. Jiao, S.-Y. Yang, D. Liu, A. Liang, Q. Xu, et al., Nat. Phys. 14 (2018) 1125–1131, http://dx.doi.org/10.1038/s41567-018-0234-5.
[56] I. Samathrakis, T. Long, Z. Zhang, H.K. Singh, H. Zhang, 2021 arXiv preprint arXiv:2105.15132.
[57] S. Husain, A. Kumar, S. Akansel, P. Svedlindh, S. Chaudhary, J. Magn. Magn. Mater. 442 (2017) 288–294, http://dx.doi.org/10.1016/j.jmmm.2017.06.127.
[58] L. Ding, J. Koo, L. Xu, X. Li, X. Lu, L. Zhao, Q. Wang, Q. Yin, H. Lei, B. Yan, Z. Zhu, K. Behnia, Phys. Rev. X 9 (2019) 041061, http://dx.doi.org/10.1103/PhysRevX.9.041061.
[59] H.Z. Yimin Ji, W. Zhang, New J. Phys. 24 (2022) 053027, http://dx.doi.org/10.1088/1367-2630/ac696c.
[60] J. Hu, S. Granville, H. Yu, Ann. Phys. 532 (2020) 1900456, http://dx.doi.org/10.1002/andp.201900456.
[61] A. Sakai, S. Minami, T. Koretsune, et al., Nature 581 (2020) 53–57, http://dx.doi.org/10.1038/s41586-020-2230-z.
[62] A. Liechtenstein, M. Katsnelson, V. Antropov, V. Gubanov, J. Magn. Magn. Mater. 67 (1987) 65–74, http://dx.doi.org/10.1016/0304-8853(87)90721-9.
[63] P.W. Anderson, Solid State Physics, vol. 14, 1963, pp. 99–214, http://dx.doi.org/10.1016/S0081-1947(08)60260-X.
[64] J. Rusz, I. Turek, M. Diviš, Phys. Rev. B, 71 174408 99–214, http://dx.doi.org/10.1103/PhysRevB.71.174408.
[65] R. Hill, Proc. Phys. Soc. A 65, 349–354, http://dx.doi.org/10.1088/0370-1298/65/5/307.
[66] M. Born, J. Chem. Phys. 7 (1939) 591–603, http://dx.doi.org/10.1063/1.1750497.
[67] V. Kanchana, G. Vaitheeswaran, A. Svane, J. Alloys Compd. 455 (2008) 480–484, http://dx.doi.org/10.1016/j.jallcom.2007.01.163.
[68] D.K. Yadav, S.R. Bhandari, G.C. Kaphle, Mater. Res. Express 7 (2020) 116527, http://dx.doi.org/10.1088/2053-1591/abcc86.
[69] Y. Suzuki, T. Katayama, S. Yoshida, K. Tanaka, K. Sato, Phys. Rev. Lett. 68 (1992) 3355, http://dx.doi.org/10.1103/PhysRevLett.68.3355.
[70] W.R. Bennett, W. Schwarzacher, W.F. Egelhoff, Phys. Rev. Lett. 65 (1990) 3169–3172, http://dx.doi.org/10.1103/PhysRevLett.65.3169.
[71] D. Weller, H. Brändle, C. Chappert, J. Magn. Magn. Mater. 121 (1993) 461–470, http://dx.doi.org/10.1016/0304-8853(93)91246-4.
[72] Y. Choe, S. Tsunashima, T. Katayama, S. Uchiyama, J. Magn. Soc. Japan 11 (1987) S1_273–276, http://dx.doi.org/10.3379/jmsjmag.11.S1_273.
[73] P.N. Argyres, Phys. Rev. 97 (1955) 334–345, http://dx.doi.org/10.1103/PhysRev.97.334.
[74] H.S. Bennett, E.A. Stern, Phys. Rev. 137 (1965) A448–A461, http://dx.doi.org/10.1103/PhysRev.137.A448.
[75] J.H. Wijngaard, C. Haas, R.A. de Groot, Phys. Rev. B 40 (1989) 9318–9320, http://dx.doi.org/10.1103/PhysRevB.40.9318.
[76] H. Feil, C. Haas, Phys. Rev. Lett. 58 (1987) 65–68, http://dx.doi.org/10.1103/PhysRevLett.58.65.